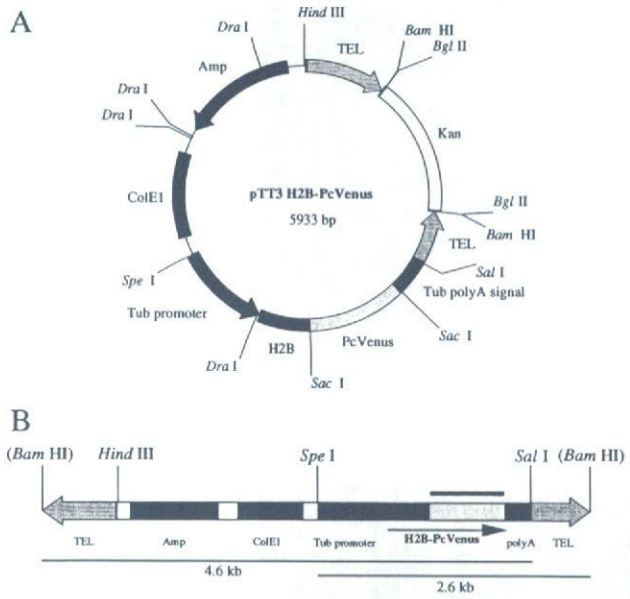

Fig. 2. Schematic diagram of pTT3 H2B–PcVenus. (A) Map of expression vector, pTT3 H2B–PcVenus. (B) Linearized pTT3 H2B–PcVenus vector. Vectors were digested with *Bam* HI before microinjection to expose telomere sequences (TEL) at both ends. Arrow shows direction of transcription. Bar indicates position of PcVenus.

telomere fragment, the (left) end adjacent to the ampicillin resistance gene of pTT3 H2B–PcVenus contained 41 (TTGGGG) repeats, whereas the other (right) end had 5 (TTGGGG) repeats (Fig. 2B). At 18 h after microinjection, fluorescence emission was intense in the nuclei of 8 among 26 cells (30.8%). Substituting the original GFP with PcVenus increased the efficiency of transformation compared with our previous results (data not shown). The nuclear localization of histone H2B–PcVenus in the transformed cells (Fig. 3A, B and C) was confirmed by staining the macro- and micronuclei with Hoechst 33342 (Fig. 3D). Fluorescent signals of PcVenus were also detected in the micronucleus (Fig. 3C, Mic) although to a much weaker extent than in the macronucleus. Fluorescent granular bodies in the cytoplasm of both transformants and untransformed cells were food vacuoles and crystal granules. We also confirmed the expression of histone H2B–PcVenus protein by Western blotting using anti-GFP antibody (Supplementary information).

3.3. Observation of histone H2B–PcVenus protein during conjugation

We examined whether the transport of macromolecules between mating cells could be directly observed by monitoring fluorescent signals from histone H2B–PcVenus protein. We initially searched cell lines for a mating partner that is easily distinguishable from transformed cells even after mating. We used the KNZcA2-11 strain (the behavioral mutant, cnrA) as the untransformed cells, as it forms heterotypic pairs when mated with transformed wild-type cells. After mixing the histone H2B–PcVenus transformants and untransformed KNZcA2-11 cells, the swimming behavior of each mating pair was examined in the high potassium solution (Hiwatashi et al., 1980) and heterotypic pairs were isolated. Mating efficiency was approximately 70%, and 20 mating pairs were observed at various times. About 30 min after the histone H2B–PcVenus transformants and untransformed KNZcA2-11 cells had mated, fluorescent signals from histone H2B–PcVenus were undetectable in the macro- and micronuclei of KNZcA2-11 cells (Fig. 4A, 0.5 h). Notably, the fluorescent signal of histone H2B–PcVenus was obvious in the macronucleus of KNZcA2-11 cells within 7 h after mixing (data not shown). At 9 h, cells reached metaphase of the first meiotic division, and the micronucleus expanded. The fluorescent signal of the macronucleus of KNZcA2-11 cells was more remarkable (Fig. 4A, 9 h). At 16 h, exconjugants underwent the second post-zygotic division. At this stage, fluorescent signals were detected in the macronuclei and in dividing micronuclei of both the histone H2B–PcVenus transformant and KNZcA2-11 cells (Fig. 4B, 16 h). Following the third post-zygotic division of micronuclei, the macronucleus was fragmented (at about 17–20 h). Thereafter, four fluorescent macronuclear anlagen appeared in both conjugants (Fig. 4B; 48 to 96 h in histone H2B–PcVenus cells; 48 and 72 h in KNZcA2-11 cells). Fluorescent signals were barely detectable in the cells derived from KNZcA2-11 96 h after mixing. On the other hand, the fragmented macronucleus and macronuclear anlagen retained significant fluorescence in the cells from the histone H2B–PcVenus transformant at the same stage (Fig. 4B, 96 h). We confirmed that the nuclear events during conjugation progressed and were completed normally in both histone H2B–PcVenus transformants and in KNZcA2-11 cells. We also confirmed that the crosses were successful by testing the post-conjugation behavioral changes of KNZcA2-11 from cnrA to wild-type. The rate of successful conjugating pairs which show the fluorescence transport was 83% at 16 h ($n=6$), 96% at 48 h ($n=27$), and 100% at 72 h ($n=20$). However, the percentage was gradually decreasing with the clonal propagation of the H2B–PcVenus transformant before conjugation, which is probably due to the heterogeneous expression of histone H2B–PcVenus (Takenaka et al., 2002).

3.4. Single-cell RT-PCR analysis

To clarify which molecules are transferred into mating untransformed cells, we performed single-cell reverse transcription-PCR (RT-PCR) to detect histone H2B–PcVenus mRNA in untransformed cells after conjugation. Some H2B–PcVenus cDNA was amplified using PcVenus-specific primers from cDNAs of H2B–PcVenus transformants at almost all time points (0, 0.5, 15, and 24 h after mixing transformant and 16B001SIIB5 cells; $n=8$), whereas no signal was evident in all untransformed 16B001SIIB5 cells (CNR mutants, cnrB) at 0 or 0.5 h (Fig. 5, PcVenus). Surprisingly, an apparent band of PcVenus fragment appeared in 3 of 8 untransformed 16B001SIIB5 cells at 15 h and in 1 of 8 cells at 24 h after mating was initiated. Cloning and sequencing the PCR product also confirmed amplification of the PcVenus fragment from 16B001SIIB5 cDNAs after mating (data not shown). When total RNA from PcVenus-positive 16B001SIIB5 cells (3

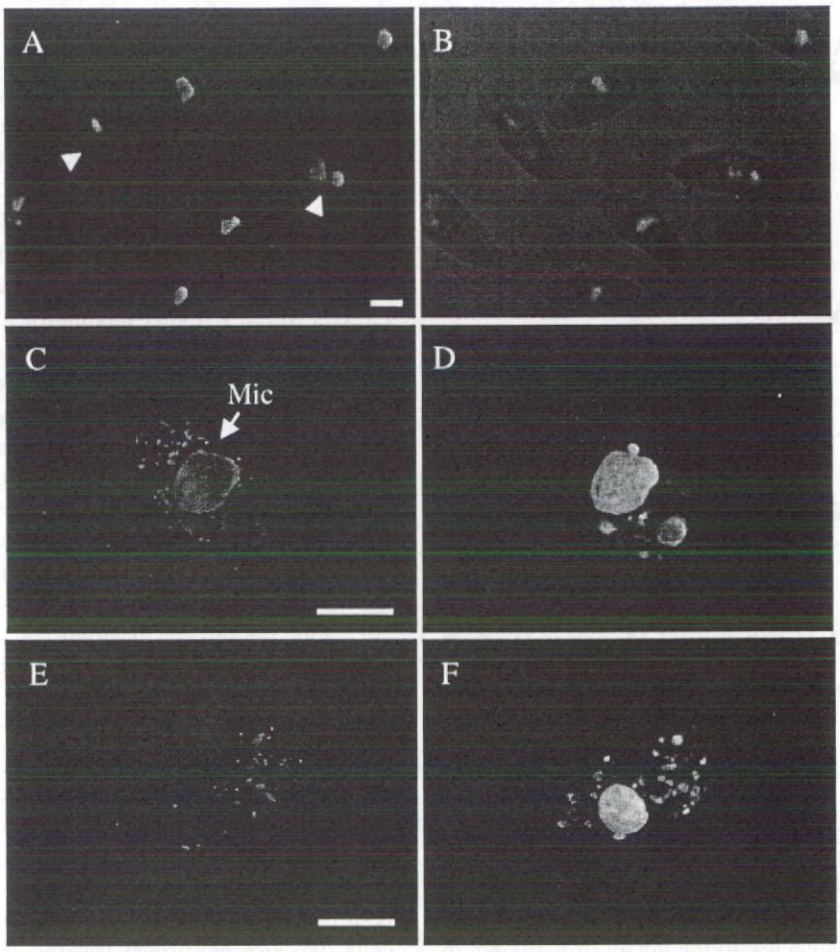

Fig. 3. Nuclear localization of histone H2B–PcVenus fusion protein in growing *P. caudatum*. (A) Vegetative cells expressing histone H2B–PcVenus. After three washes in PBS (phosphate buffered saline), cells stained with Hoechst 33258 were fixed with 1% PFA/PBS (paraformaldehyde/PBS). Arrowheads indicate amitotically dividing macronucleus. (B) Histone H2B–PcVenus fluorescence (green) overlaid onto bright-field image. (C) Images of H2B–PcVenus fluorescence and (D) Hoechst 33342 of polymer-embedded transformant clone. Histone H2B–PcVenus localized in micronucleus (Mic, arrow) and macronucleus. (E) Fluorescent and (F) Hoechst 33342 stained images of non-injected KNZcA2-11 cell. Scale bar, 50 μm.

samples at 15 h and 1 at 24 h) was used as a PCR template without reverse transcription, PcVenus signals were undetectable in all samples (data not shown). We also amplified α-tubulin cDNA from the same samples to confirm appropriate RNA extraction and cDNA synthesis from single cells (Fig. 5, α-tubulin).

4. Discussion

We cloned the *P. caudatum* histone H2B gene, and constructed an expression vector that produces H2B tagged with PcVenus to visualize cytoplasmic exchange during conjugation in real time using fluorescent microscopy. We obtained several permanent transformants in which histone H2B–PcVenus specifically localized in the macro- and micronuclei. The properties of the transformants were similar in terms of ability to divide, swimming behavior and expression of mating reactivity, to those of control sister cells that had not been microinjected with the expression vector. The morphology of the transformants did not change, indicating that the function of the expressed histone H2B–PcVenus protein remained normal. Histone H2B–PcVenus expression in each clone was stable in terms of both localization and fluorescence intensity in each cell nucleus. The clone with the most intense fluorescence and the fastest growth rate was used in the present study.

This is the first report of cloning and characterizing a histone gene in *Paramecium*, unlike the *Tetrahymena* histone proteins and their modifications, which have been extensively studied (Dou and Gorovsky, 2002; Taverna et al., 2002; Liu et al., 2004). Specific posttranslational modifications of the histone N- or C-terminal region, known as the histone code hypothesis, are considered an epigenetic control mechanism for gene expression. According to this hypothesis, histone tails can be covalently modified with a methyl group, an acetyl group, phosphate or ubiquitin, which induces specific changes in the conformation of the chromatin on which such modification occurs. For instance, the Ser-14 residue in vertebrate histone H2B becomes phosphorylated in response to several apoptotic stimuli (Cheung et al., 2003) or at DNA double-strand breaks (Fernandez-Capetillo et al., 2004). The present study revealed

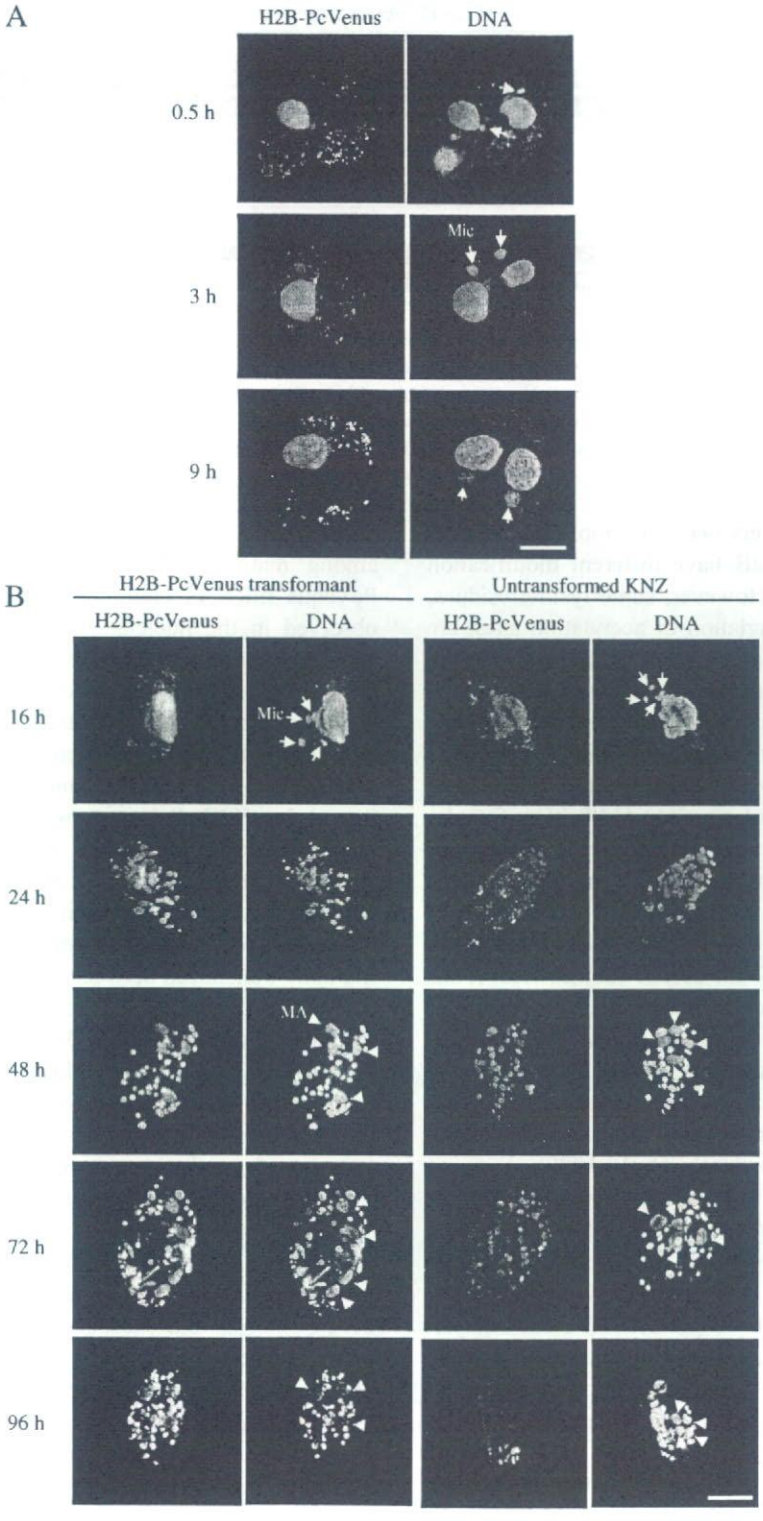

Fig. 4. Direct observation of histone H2B–PcVenus transport between mating pairs during conjugation. Histone H2B–PcVenus was localized using GFP filters (H2B–PcVenus). Nuclear DNA was stained with Hoechst 33342 and observed under UV illumination (DNA). (A) Fluorescent images of conjugating transformant cells injected with pTT3 H2B–PcVenus (left) and untransformed KNZcA2-11 (right) at 0.5–9 h after mating. (B) Cells 16–96 h after mating. About 15 h after mating, conjugating cells had separated and exconjugants were observed by fluorescent microscopy. Arrows indicate micronuclei (Mic); arrowheads indicate macronuclear anlagen (MA). Scale bar, 50 μm.

that *P. caudatum* histone H2B also possesses two serine residues at the N-terminal region (Ser-4 and -6), which are not conserved in *Tetrahymena* histone H2B. Multiple sequence alignment of histone H2Bs of *P. caudatum* and other organisms (Fig. 1) indicates that the C-terminal regions are highly conserved among vertebrates and ciliates, whereas the N-

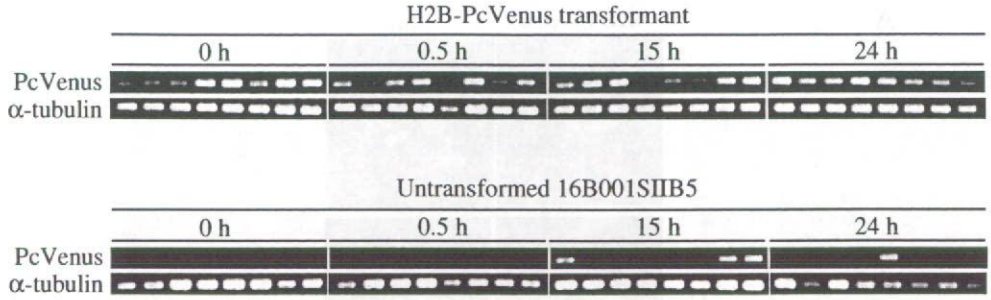

Fig. 5. Single-cell RT-PCR analysis of histone H2B–PcVenus transformed and untransformed 16B001SIIB5 (CNR mutant) cells after conjugation. Heterotypic mating pairs of transformed and untransformed cells were identified by swimming behavior, and each cell was independently harvested at 0, 0.5, 15, or 24 h after mating was initiated. After reverse transcription of total RNA, a fragment of PcVenus or α-tubulin cDNA was amplified with PcVenus- or α-tubulin-specific primers. Eight cells of H2B–PcVenus transformant or 16B001SIIB5 were independently analyzed at each time point ($n=8$). PCR products from paired H2B–PcVenus transformant and uninjected 16B001SIIB5 cell were loaded at the same lane position (0.5–24 h only). Numbers of PCR amplification cycles: 35 for PcVenus cDNA from H2B–PcVenus transformants, 40 for PcVenus from untransformed 16B001SIIB5 cells and 35 for α-tubulin cDNA.

terminal regions are notably diversified. This implies that the N-terminal regions in histone H2B have different modification sites among these organisms. However, some lysine residues, which could be potential methylation or acetylation sites, are conserved even in the N-terminal region of these H2Bs (Fig. 1). We examined the structural homology of *P. caudatum* histone H2B in terms of cross-reactivity with commercially available anti-H2B antibodies (Upstate, #07-371 and Santa Cruz Biotechnology, sc-10808) by Western blotting. However, signals at the predicted molecular weight (14.0 kDa; Supplementary information) were undetectable, indicating poor epitope homology between vertebrate and *P. caudatum* histone H2Bs.

Histone H2B tagged with PcVenus specifically localized in the macro- and micronucleus. To the best of our knowledge, this is the first description of histone localization at the vegetative stage and during conjugation in *Paramecium*. We observed fluorescent signals in the macronucleus of untransformed KNZcA2-11 cells as early as 7 h after mating (data not shown), which was a similar time course to that of conjugation rescue of the cnrC mutant (Hiwatashi et al., 1980). A curing factor of the cnrC mutant has been characterized as a soluble cytoplasmic protein with a molecular mass of about 30 kDa (Haga et al., 1983). Direct observation of the fusion protein revealed that nuclear protein or its transcript could also be exchanged during conjugation. Single-cell RT-PCR analysis indicated the H2B–PcVenus transcript in an untransformed cell 15 and 24 h after conjugation with the transformant (Fig. 5), which supports the notion that H2B–PcVenus mRNA is transported from transformed to untransformed cells. Although the number of PcVenus-positive cells after mating in RT-PCR was only 3 out of 8 at 15 h, and 1 out of 8 at 24 h (Fig. 5), several repeated RT-PCR experiments confirmed the presence of the H2B–PcVenus transcript in untransformed cells (data not shown). One reason for the low frequency of PcVenus-positive cells might be different expression levels of H2B–PcVenus transcripts in partnering transformant cells (Fig. 5). Transferred H2B–PcVenus transcript in some untransformed cells might be below detectable levels. The other reason is that the efficiency of cytoplasmic exchange and RNA transport is not the same among conjugants. In practice, we often observe heterologous efficiency of conjugation and subsequent DNA rearrangement among mating cells. We conclude that transferred H2B–PcVenus mRNAs could be one source of the fluorescence observed in the nucleus of untransformed cells. Fluorescent signals were detected in the macronucleus of untransformed cells at 7 h after mixing, which is sufficient time for translation of the transferred H2B–PcVenus mRNAs in the untransformed cytoplasm and for sufficient protein accumulation to be detectable by fluorescent microscopy. Furthermore, we assumed that H2B–PcVenus protein synthesized in the transformant cytoplasm is also the source of the fluorescent signal found in the untransformed cell, although we have not fully elucidated intercellular protein transport. The protein generally has a smaller molecular weight than RNA, and should be mutually transferred between cells as RNA during conjugation. The active export of histone protein from the nucleus to the cytoplasm has not yet been demonstrated, therefore transferred H2B–PcVenus protein might be synthesized *de novo* and unmodified. Whether transportation of H2B–PcVenus protein or mRNA depends on an active mechanism or simple diffusion from transformed to untransformed cells remains unknown.

H2B–PcVenus protein was properly localized not only in the macro- and micronuclei, but also in the macronuclear anlagen (Fig. 4B, 48–72 h) of both mating cells. These findings imply that conjugant cells share nuclear proteins from parental cells during meiosis and subsequent DNA rearrangement. Furthermore, one cell of a mating pair can affect the nuclear processes of the other by reciprocal macromolecular exchange. If many of the cytoplasmic, nuclear, and membrane proteins are mutually exchanged between mating cells, their cytoplasmic environment should be transiently synchronized. Because conjugating cells synchronously undergo two meiotic divisions and one mitotic division to produce pronuclei before pronuclear exchange, cytoplasmic exchange may play a role for generation of synchronization of various cellular events including meiotic and mitotic divisions, the exchange of pronuclei and the subsequent disengagement of mating cells.

The function of small RNAs in genome rearrangement events such as the elimination of micronuclear-specific sequences has been studied in *Tetrahymena* (Mochizuki et al., 2002; Mochizuki and Gorovsky, 2004). Heterogeneous small

RNAs are specifically expressed in *Tetrahymena* before chromosome rearrangement during conjugation. Small RNAs are also involved in the genome rearrangement of *P. tetraurelia* (Garnier et al., 2004). We are currently investigating the possibility of small RNA transfer between mating partners during conjugation using the single-cell RT-PCR established in the present study. Further analysis of cytoplasmic exchange in *Paramecium* would facilitate deeper understanding of the overall mechanism of genome remodeling and of synchronized conjugation.

Acknowledgements

This study was supported in part by the Special Coordination Funds for Promoting Science and Technology of the Ministry of Education, Culture, Sports, Science and Technology of Japan (H. Mizuno), matching research funds from NIAS & NEC Soft, Ltd. (H. Masuda and H. Mizuno), and funds from the University of Tsukuba (Y. Takenaka and Y. Mitsui).

Appendix A. Supplementary information

A. Immunoblot analysis of *P. caudatum* cellular lysate using anti-GFP antibody (BD Clontech #632459).

Lane 1, untransformed cells; lane 2, transformants expressing H2B–PcVenus.

B. Immunoblot analysis using anti-histone H2B antibody (Upstate #07-371).

Lane 1, *E. coli* lysate overexpressing *P. caudatum* histone H2B; lane 2, untransformed cells; lane 3, transformant expressing H2B–PcVenus. Arrowhead indicates predicted size of H2B–PcVenus protein.

C. Immunoblot analysis detected by anti-histone H2B antibody (Santa Cruz #sc-10808).

Lane 1, *E. coli* lysate overexpressing *P. caudatum* histone H2B; lane 2, untransformed cells; lane 3, transformant expressing H2B–PcVenus. Arrowhead indicates predicted size of H2B–PcVenus protein.

Appendix B. Supplementary data

Supplementary data associated with this article can be found, in the online version, at doi:10.1016/j.gene.2007.02.013.

References

Aury, J.M., et al., 2006. Global trends of whole-genome duplications revealed by the ciliate *Paramecium tetraurelia*. Nature 444, 171–178.

Cheung, W.L., et al., 2003. Apoptotic phosphorylation of histone H2B is mediated by mammalian sterile twenty kinase. Cell 113, 507–517.

Dou, Y., Gorovsky, M.A., 2002. Regulation of transcription by H1 phosphorylation in *Tetrahymena* is position independent and requires clustered sites. Proc. Natl. Acad. Sci. U. S. A. 99, 6142–6146.

Fernandez-Capetillo, O., Allis, C.D., Nussenzweig, A., 2004. Phosphorylation of histone H2B at DNA double-strand breaks. J. Exp. Med. 199, 1671–1677.

Garnier, O., Serrano, V., Duharcourt, S., Meyer, E., 2004. RNA-mediated programming of developmental genome rearrangements in *Paramecium tetraurelia*. Mol. Cell. Biol. 24, 7370–7379.

Haga, N., Saimi, Y., Takahashi, M., Kung, C., 1983. Intra- and interspecific complementation of membrane-inexcitable mutants of *Paramecium*. J. Cell Biol. 97, 378–382.

Hiwatashi, K., Haga, N., Takahashi, M., 1980. Restoration of membrane excitability in a behavioral mutant of *Paramecium caudatum* during conjugation and by microinjection of wild-type cytoplasm. J. Cell Biol. 84, 476–480.

Kanda, T., Sullivan, K.F., Wahl, G.M., 1998. Histone-GFP fusion protein enables sensitive analysis of chromosome dynamics in living mammalian cells. Curr. Biol. 8, 377–385.

Kimura, H., Cook, P.R., 2001. Kinetics of core histones in living human cells: little exchange of H3 and H4 and some rapid exchange of H2B. J. Cell Biol. 153, 1341–1353.

Liu, Y., Mochizuki, K., Gorovsky, M.A., 2004. Histone H3 lysine 9 methylation is required for DNA elimination in developing macronuclei in *Tetrahymena*. Proc. Natl. Acad. Sci. U. S. A. 101, 1679–1684.

Mochizuki, K., Gorovsky, M.A., 2004. Conjugation-specific small RNAs in *Tetrahymena* have predicted properties of scan (scn) RNAs involved in genome rearrangement. Genes Dev. 18, 2068–2073.

Mochizuki, K., Fine, N.A., Fujisawa, T., Gorovsky, M.A., 2002. Analysis of a piwi-related gene implicates small RNAs in genome rearrangement in *Tetrahymena*. Cell 110, 689–699.

Nagai, T., Ibata, K., Park, E.S., Kubota, M., Mikoshiba, K., Miyawaki, A., 2002. A variant of yellow fluorescent protein with fast and efficient maturation for cell-biological applications. Nat. Biotechnol. 20, 87–90.

Takenaka, Y., Haga, N., Harumoto, T., Matsuura, T., Mitsui, Y., 2002. Transformation of *Paramecium caudatum* with a novel expression vector harboring codon-optimized GFP gene. Gene 284, 233–240.

Taverna, S.D., Coyne, R.S., Allis, C.D., 2002. Methylation of histone h3 at lysine 9 targets programmed DNA elimination in *Tetrahymena*. Cell 110, 701–711.

Original

Paramecium as a bioassay system for elucidation of cytotoxicity and biocompatibility of nanoparticles: effects of carbon nanofibers on proliferation and survival

Nobuyuki HAGA[1]* and Koichi HANEDA[2]

[1]*Department of Biological Technology,* [2]*Department of Information Technology and Electronics, Senshu University of Ishinomaki, Ishinomaki, Miyagi 986-8580, Japan*

SUMMARY

Carbon nanofibers (CNF), composed of carbon nanotubes, are a recent technological advance with wide applications in nano-engineering fields including biotechnology and biomedicine. However, little is known about the environmental effects of CNF, or their potential danger to human health. To elucidate the safety of CNF, we examined the cytotoxicity of CNF in *Paramecium*. In this study we considered the cytotoxicity effect of CNF in two categories of cellular properties, cell survival and cell proliferation. We show that CNF are ingested and concentrated as efficiently as nutritive bacteria by paramecia, revealing a means by which CNF could be introduced into the food webs of aquatic ecosystems. Clear cytotoxicity of CNF was detected in survival tests by extracellular application at extremely high concentration (up to 50 mg/ml) in culture medium containing nutritive bacteria. Contrary to this effect, no cytotoxicity was detected in survival tests using the modified Dryl's solution (K-DS) that is used as a buffered saline of culture medium. The cytotoxicity of CNF suggests an interaction between CNF and the components in culture medium or their metabolic products produced by digestion of components in culture medium. Another cytotoxicity effect was detected in proliferative activity test at lower concentrations of CNF (up to 500 μg/ml). The cytotoxicity on proliferative activity was reversible and recovery occurred within 24 hours after removal of CNF. Our results suggest that *Paramecium* is useful for a bioassay of nanoparticle cytotoxicity. For the elucidation of safety of CNF we have to examine both the optimum concentration of CNF and co-existing biomaterials in a test solution. In conclusion, CNF have a high potential for cytological and biomedical application under precise control of concentration.

*Corresponding author
Tel: +81-225-22-7716, Fax: +81-225-22-7746
E-mail: haga@isenshu-u.ac.jp
Received:5 March 2006; Accepted:10 September 2007

INTRODUCTION

The safety of materials to living organisms usually depends upon particle size: substances that are safe in macroscopic quantities can become dangerous when reduced to microscopic particles (Brown et al, 2001). As the behavior of nanoparticles in the environment and in cells is not well understood, it is important to establish an experimental system in which to assess the effects of nanoparticles on the environment and on living organisms.

Paramecium, a ciliated eukaryotic unicellular organism that lives in fresh water, has several features that make it a potentially valuable model to assay the cytotoxicity of environmental agents (Rajini et al, 1989, Smith-Sonneborn et al, 1983, 1986): they can ingest both soluble molecules and many different types of particle, including polyethylene particles, India ink, iron filings and sand, by phagocytosis, and they show very stable cellular functions such as phagocytosis, cell division and swimming behavior. In this study, we examine the use of *Paramecium* as a bioassay for evaluating the cytotoxicity of nanoparticles and have established a standard experimental method that enables micro liter-sized assays.

The CNF used in this experiment have a structure of hollow graphitic tubules of nanometer dimensions, and are comprised of coaxial tubes of helically arranged carbon-hexagon sheets. Typically, their diameters ranged from 2 to 20 nm, and they were several micrometers in length (Iijima, 1991).

MATERIALS AND METHODS

Cells and culture medium

Paramecium caudatum, syngen 3 was used in this study. They were grown at 25°C in a culture medium containing 1.25% (w/v) fresh lettuce juice diluted with K-DS (Dryl's solution (Dryl, 1959) modified by substituting KH_2PO_4 for NaH_2PO_4, pH 7.0 (Yanagi, 1987)) and inoculated with *Klebsiella pneumoniae* one day before use (Hiwatashi, 1968).

CNF production

CNF were provided by Prof. K. Tohji (Tohoku University, Japan). They were produced in a conventional flow reactor system (Rodriguez, 1993) in which a hydrocarbon/carrier-gas mixture (C_2H_4/H_2 (4:2)) was pyrolysed at 873 K for 4 hours in the presence of powdered Ni catalyst. The catalyst was positioned in an Al_2O_3 boat and set in a quartz tube assembled in a horizontal tube furnace; it had been reduced in advance in a 10% H_2/He stream for 2 hours at 873 K.

As the CNF inevitably contain an appreciable amount of metallic elements, such as Ni, a purification process is vital to both fundamental studies and potential applications of the material (Ebbesen et al, 1994; Tohji, 1996). The CNF used in this study were purified by hydrochloric acid treatment (Tohji et al, 1996).

CNF ingestion

CNF were washed twice with K-DS with centrifugation at 10,000 rpm for 5 min. The washed CNF were suspended at a concentration of 100 mg/ml in K-DS. Paramecia were washed twice with K-DS by a hand centrifuge and suspended in K-DS at the cell density of about 4,000 cells/ml. Then, 40 µl of the CNF suspension was mixed with an equal volume of the cell suspension and the mixture was incubated at 25°C. The paramecia were periodically isolated from the mixture with a hand-made glass micropipette and put into a drop of 2.5%(w/v) methyl cellulose dissolved in K-DS on a glass slide. Photographs were taken under a light microscope (ZEISS AX10) by a digital camera (Nikon, DS-5Mc).

Cytotoxicity test of CNF

A CNF suspension was prepared in an autoclaved glass depression slide with an autoclaved microchip by mixing CNF stock suspension with either K-DS or fresh culture medium. Then, a single paramecium was added into 100 µl of the CNF mixture with a hand-made glass micropipette under a binocular microscope. The CNF suspension with the paramecium was incubated at 25°C.

Capillary culture method

We developed a small-sized bioassay using a glass capillary (0.6 mm inside diameter and 35 mm length) by modification of the method (Haga and Hiwatashi, 1981). Twenty µl of a CNF suspension containing paramecia was put on a glass depression slide and then the suspension was drawn into a capillary by capillary action. The capillary was placed in a laboratory dish with a sheet of wet paper. This method allows a one-week incubation at 25°C without any serious problem of evaporation of the medium.

Statistic analysis

Statistical analysis of the data from the dose-effect experiments was performed using the Dunnett test (Graph pad Prism 4).

RESULTS

Ingestion of CNF and food vacuole formation

Paramecia ingest nutritive bacteria via the buccal cavity and concentrate the bacteria, together with a small amount of fluid, in food vacuoles. CNF-containing food vacuoles are shown in Figure 1a and 1b. Immediately after initial contact with CNF Paramecia began to ingest CNF by forming a food vacuole. CNF particles were concentrated in each food vacuole. No CNF particle that escaped from a food vacuole into cytoplasm was detected by a light microscope observation.

Effect of CNF on non-proliferating cell survival

Before testing the cytotoxicity of CNF, we examined experimental conditions to prepare homogeneous dispersion of CNF suspension in K-DS. By varying the concentrations of CNF and the time of sonication, we confirmed that a homogeneous suspension of CNF could be obtained in up to a concentration of 50 µg/ml in K-DS for 20 min sonication.

Paramecia do not undergo proliferation when incubated in a bacteria-free solution. The survival of non-proliferating paramecia was examined by using a capillary culture with 20 µl of CNF suspension in K-DS. In the presence of 50 mg/ml of CNF, all of the tested cells remained alive through-

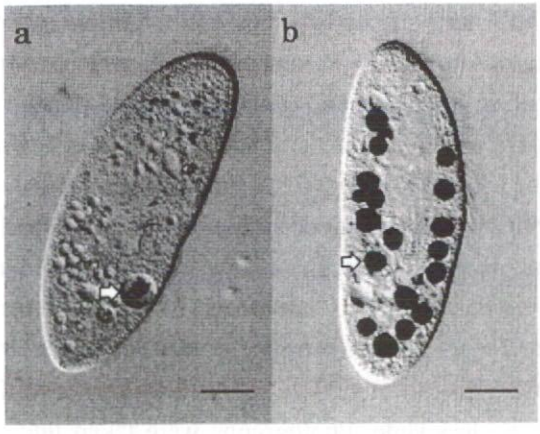

Fig. 1. A photograph of a living *Paramecium* ingesting CNF. a: At 1 min after the initiation of incubation in a CNF suspension (50 mg/ml), a cell was isolated in 2.5% (w/v) methyl cellulose dissolved in K-DS and mounted on a glass slide. Then, about 5 min later, a photograph was taken with a digital camera (Nikon, DS-5Mc) attached to a light microscope (ZEISS AX10). A white arrow shows aggregating CNF particles in a food vacuole. b: A photograph was taken at 20 min after the initiation of incubation in the CNF suspension. Black particles, one of which is shown by a white arrow, indicate CNF-containing food vacuoles. Bar is 30 µm.

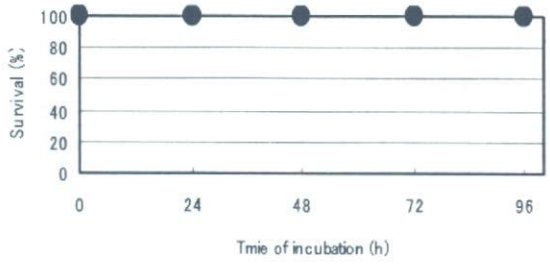

Fig. 2a. Survival rates of non-proliferating paramecia in a 50 mg/ml CNF suspension. The abscissa shows length of time of incubation in the CNF suspension, and the ordinate shows the mean percentage of cells surviving up to 96 h after the initiation of incubation (n=6).

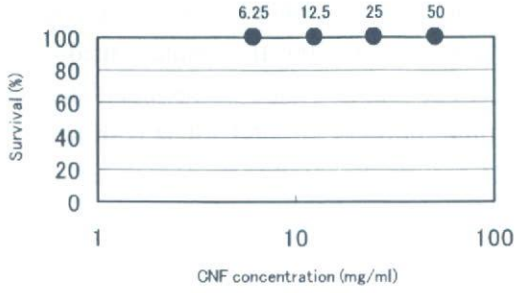

Fig. 2b. Effect of different doses of CNF on survival of non-proliferating paramecia. The abscissa shows the amount of CNF suspended in K-DS. Scale of abscissa was shown by logarithm. The ordinate shows the mean percentage of cells surviving up to 96 h after the initiation of incu-

out the period of 96 hours incubation, without any noticeable detrimental response to CNF exposure (Fig. 2a). No cytotoxicity was detected over a range of CNF concentrations up to 50 mg/ml in non-proliferating paramecia (Fig. 2b).

Effect of CNF on proliferation

The effect of CNF on the proliferation of paramecia was tested in fresh culture medium containing nutritive bacteria in a glass depression slide culture. A single cell was suspended in 200 µl of the CNF suspension (50 mg/ml) and then was kept at 25℃. Under these conditions, during the first 24 hours the paramecia underwent cell division once, but their daughter cells gradually lost the ability to swim and, after 48 hours of incubation, more than 95% died. On the other hand, cells in the control culture continued cell divisions during 48 hours of incubation (Fig. 3a).

We examined cytotoxicity effect of CNF at

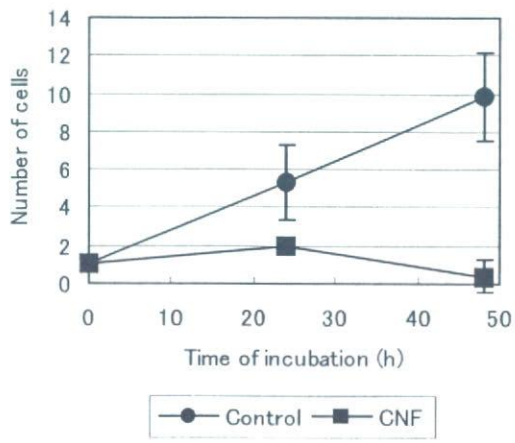

Fig. 3a. Survival of proliferating paramecia cultured in a CNF suspension. The abscissa shows time after the initiation of incubation and the ordinate shows the mean number of surviving cells in fresh culture medium containing nutritive bacteria and 50 mg/ml CNF (n=6). Control means the culture containing 0 mg/ml of CNF (n=6).

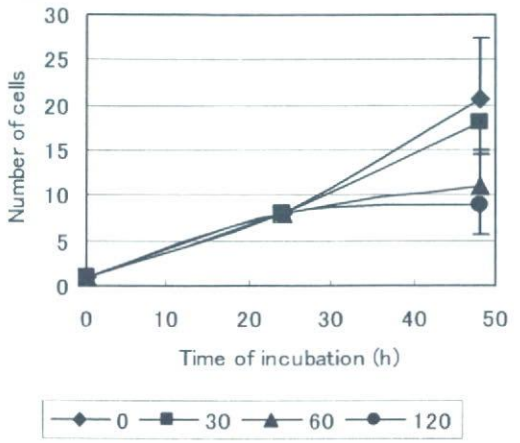

Fig. 3b. The time course of proliferation in different concentrations of CNF. The mean numbers of cells in fresh culture medium containing nutritive bacteria are shown (n=6). Diamond, 0; square, 30; triangle, 60; and circle, 120 µg/ml CNF. The abscissa shows time after the initiation of incubation and the ordinate the mean number of living

lower amount of CNF suspension. A single cell was suspended in 200 µl of culture medium containing bacteria in a glass depression slide culture. The time course of the CNF effect is shown in Fig. 3b. During the first 24 hours in bacteria-containing culture medium, CNF did not inhibit proliferation at any concentration. However, during the second 24 hours incubation, 60 and 120 µg/ml of CNF inhibited cell division.

The dose effect of CNF on proliferation at 48 hours after incubation is shown in Fig. 4. The mean number of cells at 30 µg/ml of CNF was about 80% of that of the control culture (Dunnett, $P<0.05$). At 60 µg/ml of CNF, the mean number of cells decreased to about 40% of the control (Dunnett, $P<0.01$), and remained at this level as the concentration of CNF increased. Thus, no dose effect was observed above 60 µg/ml of CNF.

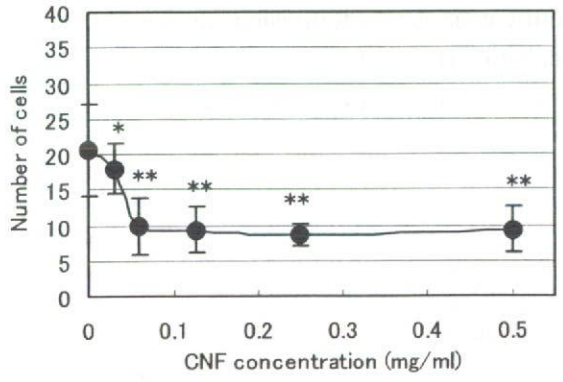

Fig. 4. Dose effect of CNF on proliferation. The abscissa shows the concentration of CNF and the ordinate the mean number of surviving cells at 48 h after the initiation of incubation. Bars show the standard deviation and * indicates a significant statistical difference at $P<0.05$ (Dunnett test) and ** at $P<0.01$ (Dunnett test) (n=6).

Reversibility of the cytotoxicity effect of CNF

The reversibility of cytotoxicity of CNF was examined by transferring paramecia cultured for 48 hours in various CNF concentrations to CNF-free fresh culture medium in a glass depression slide. As shown in Fig. 5, at 30, 60 and 125 µg/ml of CNF, the mean number of cells at 48 hours incubation recovered to control levels (CNF: 0 µg/ml). At 250 and 500 µg/ml, the mean number of cells did not recover fully, although statistical analysis showed no significant differences among the CNF concentrations (Dunnett, $P<0.09$ at 250 µg/ml).

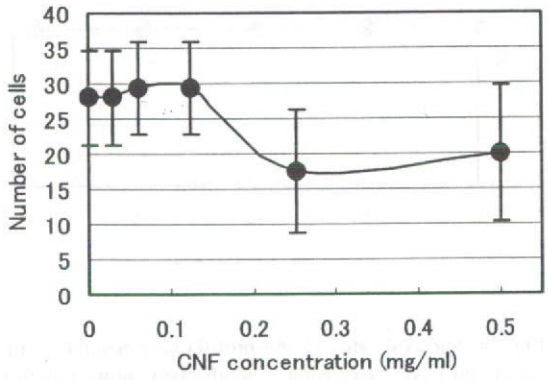

Fig. 5. Recovery of proliferative activity after removal of CNF. The abscissa shows the concentration of CNF and the ordinate the mean number of surviving cells at 48 h after the initiation of incubation. Bars indicate standard deviations (n=6).

DISCUSSION

The health risks to humans and other organisms from exposure to nanoparticles in the environment are one of the most important concerns regarding the use of these potentially valuable materials. The *Paramecium* bioassay system described here provides a useful means by which to determine the cytotoxicity of environmental and ingested CNF.

Paramecia play an important role in food webs in aquatic ecosystems. They ingest diverse bacteria growing in water (Taylor, 1979) and, in turn, are

eaten by other protozoa such as amoebas, didinia and other metazoan animals or their larvae (Porter et al, 1979; Taylor, 1980). Thus, CNF could move into food webs of aquatic ecosystems following ingestion by paramecia. The speed of a CNF-containing food vacuole formation and the maximum number in a cell were similar to those observed after ingestion of nutritive bacteria (data not shown)

Two types of nuclear division occur in *Paramecium*: mitotic nuclear division performed by the micronucleus, and amitotic division by the macronucleus. For the purposes of this article, the cells incubated in K-DS are referred to as "non-proliferating" cells.

At the beginning of this study, we set two categories of cellular properties for an assessment of the cytotoxicity effect of CNF. One is the property of cell survival and the other cell division. For cell survival tests we used the buffered saline, K-DS, and examined survival ratio and swimming behavior. In non-proliferating paramecia, CNF had no cytotoxicity effect on both cellular properties in all experiments performed in this study.

However, we have found strong cytotoxic effect of CNF in the cell division tests. In this test we used culture medium containing lettuce juice and nutritive bacteria as described in "Materials and Methods". The cytotoxic effect of CNF was observed in both properties of cell survival and cell division. At 50 mg/ml of CNF, cytotoxic effect was detected in the property of cell division during the initial 24-hour incubation and no effect on the property of cell survival. In the following 24-hour incubation, however, cytotoxic effect was detected in the property of cell survival, too.

We considered the possibility of causal relation of CNF effect on the property of cell survival. The simplest case is the inhibition of energy source uptake by CNF. But, it is hard to assume this case because, under our experimental conditions, paramecia can survive more than 1 week without any nutrient biomaterials indicating that the energy pool of cytoplasm is enough for surviving in the period of experiments performed in this study. However, an energy source uptake under the presence of CNF is remained to estimate experimentally.

An alternative possibility is the production of hazardous chemical substances by interaction between the metabolic products of culture medium and CNF. At this moment we have no information about chemical compositions of the culture medium. However, one candidate of the hazardous chemical substances is suggested by the following observation. One of the remarkable characteristics observed regarding cytotoxicity of CNF was the cessation of ciliary movement on the cell surface of proliferating paramecia. Ciliary movement in paramecia is essentially controlled by membrane potential (Dunlap, 1977; Kung and Saimi, 1982). Because the control of membrane potential is dependent on several kinds of ion channels (Kung and Saimi, 1982), chemical substances that affect ion channel functions will be one of target molecules to understand cytotoxicity of CNF.

Alternative experimental approach to the molecular mechanisms of CNF cytotoxicity is the use of complete synthetic culture medium in a cell division test. In this experiment we could systematically change chemical compositions in culture medium, so that the cytotoxicity of CNF control.

As shown in Fig. 4, the dose effect of CNF cytotoxicity was biphasic: at lower concentrations (from 30 to 60 μg/ml of CNF), a dose dependency was observed, while the effect appeared independent of dose at higher concentrations (from 60 to 500 μg/ml of CNF). The number of cells in culture medium depends on both the number of cell divisions and the number of cell death during cultivation. To obtain precise information about the contribution of cell division and cell death we have to perform a single cell isolation line culture under the presence of CNF after every cell division in

future experiments.

Our findings indicate that the effect of CNF on living organisms might not be as simple as previously predicted. We anticipate the presence of some complexity involving the molecular interactions between CNF and intracellular chemicals, which, in turn, may have harmful effects on cells.

In summary, the *Paramecium* bioassay system reveals that it is important to distinguish the property of cell division and cell survival in the elucidation of CNF cytotoxicity. As our studies have indicated, developing the appropriate regulatory guidelines to ensure the safety of nanotechnology will require biochemical examination and identification of chemical substances that interact with and modulate CNF cytotoxicity.

ACKNOWLEDGMENTS

Research was performed under Health and Labor Sciences Research Grants for Research on Risk Assessment of Chemical Substances: "Development of Visualization Method of Dynamical Motion Behavior of Nanoparticles in the Internal Body (H18-Chem-General-006)" from Ministry of Health, Labor and Welfare of Japan.

REFERENCES

Brown, D. M., Wilson M. R., MacNee W., Stone V., and Donalodson K. (2001) Size-dependent proinflammatory effects of ultrafine polystyrene particles: A role for surface area and oxidative stress in the enhanced activity of ultrafines. Toxicology and Applied Pharmacology 175, 191-199.

Dunlap, K. (1977) Localization of calucium channels in *Paramecium caudatum*. J. Physiol. 271, 119-133.

Dryl, S. (1959) Antigenic transformation in *Paramecium aurelia* after homologous antiserum treatment during autogamy and conjugation. J. Protozool., 6 (Suppl.), 25.

Haga, N. and Hiwatashi, K. (1981) A protein called immaturin controlling sexual immaturity in *Paramecium*. Nature 289, 177-179.

Hiwatashi, K. (1968) Determination and inheritance of mating type in *Paramecium caudatum*. Genetics 58, 373-386.

Iijima, S. (1991) Helical microtubules of graphitic carbon. Nature 354, 56-58.

Kung, C. and Saimi, Y. (1982) The physiological basis of taxis in *Paramecium*. Ann. Rev. Physiol. 44, 519-534.

Porter, K.G., Pace, M.L. and Batte, J. F. (1979) Ciliate protozoans as links in fresh-water planktonic food chains. Nature 277, 563-565.

Rajimi, P. S., Krishnakumari, M. K., and Majumder, S. K. (1989) Cytotoxicity of certain organic solvents and organophosphorus insecticides to the ciliated protozoan *Paramecium caudatum*. Microbios 59, 157-163.

Rodriguez, N.M. (1993) A review of catalytically grown carbon nanofibers. J. Matter Res., 8, 3233-3250.

Smith-Sonneborn, J., Palizzi, R.A., McCann, E.A., and Fisher, G.L. (1983) Bioassay of genotoxic effects of environmental particles in a feeding ciliate. Environ Health Perspect. Sep; 51, 205-210.

Smith-Sonneborn, J., Leibovitz, B., Donathan, R., and Fisher, G.L. (1986) Bioassay of environmental nickel dusts in a particle feeding ciliate. Environ. Mutagen. 8 (4), 621-626.

Taylor, W.D. (1979) Overlap among cohabiting ciliates in their growth responses to various prey bacteria Can. J. Zool., 57, 949-951.

Taylor, W.D. (1980) Observation on the feeding and growth of the predacious oligochaete *Chaetogaster langi* on ciliated protozoa. Trans. Am. Microsc. Soc., 99, 360-367.

Tohji, K., Goto, T., Takahashi, H., Shinoda, Y.,

Shimizu, N., Jeyadevan, B., Matsuoka, I., Saito, Y., Kasuya, A., Ohsuna, T., Hiraga, K., and Nishina, Y. (1996) Purifying single-walled nanotubes. Nature 383, 679.

Yanagi, A. (1987) Positional control of the fates of nuclei produced after meiosis in *Paramecium caudatum*: analysis by nuclear transplantation. Dev. Biol. 122, 535-539.

Fullerenes, Nanotubes, and Carbon Nanostructures, 16: 114–125, 2008

ISSN 1536-383X print/1536-4046 online
DOI: 10.1080/15363830801887992

Carbohydrate Coating of Carbon Nanotubes for Biological Recognition

Tsukasa Akasaka and Fumio Watari

Department of Biomedical Materials and Engineering, Graduate School of Dentistry, Hokkaido University, Sapporo, Japan

Abstract: We have demonstrated that multi-walled carbon nanotubes (MWNTs) coated with a carbohydrate-carrying polymer for use as biological recognition signals can be easily prepared by a non-covalent method via hydrophobic interactions. Fluorescence observation by confocal laser scanning microscopy showed that the carbohydrate-carrying polymers were densely localized around the MWNTs. To evaluate biological recognition affinity, interactions of the MWNTs with lectins were examined by binding tests. The resultant MWNTs were found to acquire a selective binding affinity to the corresponding lectin without a non-specific interaction. On the other hand, bare MWNTs non-specifically interacted with lectins. These results showed that the MWNTs coated with a carbohydrate-carrying polymer have biological recognition signals. Modification of carbon nanotubes with various carbohydrate chains will be a useful protocol for molecular designs of biomaterials, nanoarchitecture and biosensors.

Keywords: Carbon nanotubes, carbohydrate, surface modification, recognition, lectin

INTRODUCTION

Carbon nanotubes (CNTs) have been attracting considerable attention because of their unique physical properties and potential for a variety of applications. Modifications of CNTs by covalent and non-covalent methods have been examined in recent studies (1–6). It is interesting to decorate the open end

Received 9 October 2007, Accepted 2 January 2008
Address correspondence to Tsukasa Akasaka, Department of Biomedical Materials and Engineering, Graduate School of Dentistry, Hokkaido University, 060-8586 Sapporo, Japan. E-mail: akasaka@den.hokudai.ac.jp

or the outer surface of CNTs with biological molecules such as DNA (7, 8), protein (9, 10), enzyme (11, 12), poly- and mono-saccharide (13–18) and others (19, 20). DNA molecules adsorbed on the surface of CNTs via nonspecific interactions have been observed (7). Streptavidin has also been found to adsorb on the surface of CNTs presumably via hydrophobic interactions (9).

Biological functions of carbohydrate chains of glycolipids and glycoproteins have attracted much attention in recent years. Carbohydrate chains are involved in various recognition phenomena, such as fertilization, cell adhesion, tissue formation, antigen-antibody reaction, cancer metastasis and infection of viruses and bacteria (21). More attention has recently been paid to synthetic polymers with pendant carbohydrate chain moieties for use as biological recognition signaling molecules (22). Carbohydrate-carrying polymers have been used as cell-specific culture substrata, in human vaccines, for tumor diagnosis, as probes for receptors, and in targeted drug delivery systems (23–27). These applications are based on biological recognition phenomena, that is, specific interactions between carbohydrates on the polymers and proteins (28–30).

However, no facile method for incorporating carbohydrate chains as recognition signaling molecules into CNTs has been reported. Here we describe a simple method for surface modification of CNTs with carbohydrate chains as recognition signaling molecules. In this study, we used commercially available lactose-carrying polystyrene (PVLA) (31–33), which has both pendant β-galactose moieties for use as recognition signaling molecules and a polystyrene backbone that can be adsorbed onto the surface of CNTs via hydrophobic interactions.

EXPERIMENTAL PROCEDURES

Materials

Poly-(*N*-*p*-vinyl benzyl-*O*-β-D-galactosyl-D-gluconamide) [lactose-carrying polystyrene (PVLA); MW: 5×10^4] and FITC-labeled PVLA were purchased from Seikagaku Corp. (Tokyo, Japan). Rhodamine-labeled *Ricinus communis* agglutinin lectin (Rhod-RCA_{120}, β-galactose-specific lectin) and rhodamine-labeled concanavalin A (Rhod-ConA, α-glucose- or α-mannose-specific lectin) were purchased from VECTOR Laboratories, Inc. (Burlingame, Calif., USA).

Multi-walled carbon nanotubes (MWNTs) used in this study were obtained from two different sources: NanoLab (Brighton, Mass., USA) and MTR Co., Ltd. (Ohio, USA). MWNTs from NanoLab (30-MWNTs; about 30 nm in average diameter) were produced by the chemical vapor deposition (CVD) method, whereas MWNTs from MTR Co. (200-MWNTs; about 200 nm in average diameter) were produced by the arc discharge method. The raw MWNTs were refluxed in 6 N HCl solution and then washed

thoroughly with deionized water and completely dried. 30-MWNTs contain <20% amorphous carbon and 200-MWNTs contain <15% amorphous carbon as the dominant impurity. Typical SEM images of the purified MWNTs are shown in Figure 1.

Preparation of the MWNTs Coated with a Carbohydrate-carrying Polymer

MWNTs material was dispersed in 10 mM phosphate-buffered saline (PBS (+), pH 7.2, 0.5 mL) at a concentration of 50 mg/L by ultrasonication for 15 min. A sufficient amount of PVLA was added to the MWNTs solution to result in a 2% solution by weight, which was then ultrasonicated for 15 min. After 1 h of incubation at room temperature, the mixture was centrifuged (13,000 *g*, 10 min). The aggregated MWNTs were carefully washed three times with PBS and two times with deionized water to remove the unadsorbed polymer.

Interactions with Lectins

A small portion of the MWNTs coated with FITC-PVLA was suspended in 10 mM phosphate-buffered saline (PBS (+), pH 7.2, 0.5 mL). Rhod-RCA_{120} (or Rhod-ConA) was added to a final concentration of 450 nM, and the mixture was then incubated for 1 h at room temperature. After incubation, the mixture was centrifuged (13,000 *g*, 10 min). The aggregated MWNTs were carefully washed three times with PBS and two times with deionized water to remove the uninteracted lectin.

To observe non-specific interactions with lectins, a small portion of bare MWNTs was suspended in PBS. Rhod-RCA_{120} (or Rhod-ConA) was added to a final concentration of 450 nM. After 1 h of incubation at room temperature, the mixture was centrifuged (13,000 g, 10 min). The aggregated MWNTs

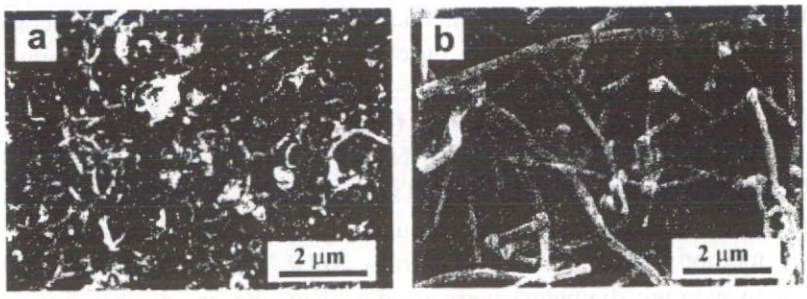

Figure 1. SEM images of the purified MWNTs. a: 30-MWNTs, b: 200-MWNTs.

were carefully washed three times with PBS and two times with deionized water to remove the unadsorbed lectin.

Scanning Electron Microscopy (SEM)

A HITACHI S-4000 scanning electron microscope (HITACHI Instruments, Inc., Tokyo, Japan) was used for SEM.

Fourier Transform Infrared Spectroscopy (FT-IR)

IR absorption spectra were obtained using a JASCO FT/IR-300E fourier transform infrared spectrometer (JASCO, Tokyo, Japan) in the transmission mode on pressed MWNTs pellets mixed with KBr.

Confocal Laser Scanning Microscopy (CLSM)

For CLSM, a small drop of sample solution was placed onto a glass slide, and the solution was covered with a cover glass to prevent evaporation of the solution. CLSM was performed using a Carl Zeiss LSM 410 Axiovert microscope (Carl Zeiss, Oberkochen, Germany) in the transmitted light mode and the fluorescence mode with a 20 × objective at zoom factor 4.8. FITC was excited with a 488-nm argon beam, and emission was collected between 515 and 565 nm. Rhodamine was excited with a 543-nm He-Ne beam, and emission was collected beyond 590 nm. Two different images were acquired from each laser line with green and red colors from FITC and rhodamine, respectively.

RESULTS AND DISCUSSION

Preparation of MWNTs Coated with Carbohydrate-carrying Polymer

In the method reported by O'Connell et al. (34), formation of chemical bonds was substituted by wrapping single-walled carbon nanotubes (SWNTs) in macromolecules such as poly(vinylpyrrolidone) and polystyrene sulfonate molecules. On the basis of their reported method, we used lactose-carrying polystyrene (PVLA) as a model carbohydrate-carrying polymer in this work. The procedure used for coating 30-MWNTs with PVLA was as follows. PVLA and 30-MWNTs material were put into water and ultrasonicated for 15 min. After 1 h of incubation at room temperature, the mixture was centrifuged. The aggregated 30-MWNTs were carefully washed with PBS and deionized water to remove the unadsorbed polymer.

Infrared transmission spectra of 30-MWNTs, the 30-MWNTs coated with PVLA, and PVLA were obtained to observe the bonding between 30-MWNTs and PVLA (Figure 2). Compared with the spectrum of 30-MWNTs (Figure 2a), new peaks at around 3430, 2920 and 1640 cm^{-1} on the spectrum of the 30-MWNTs coated with PVLA (Figure 2b) were observed. These peaks were assigned to -OH, $-CH_2$ and C=O, respectively, functional groups derived from PVLA. The presence of these new peaks indicated that there was still a significant amount of PVLA left in the aggregated 30-MWNTs after washing, suggesting that the MWNTs interacted strongly with PVLA.

To observe the interaction between the MWNTs and PVLA more directly, we performed fluorescence CLSM (8, 20) using an FITC-labeled carbohydrate-carrying polymer. In this experiment, small aggregations of the MWNTs, scattered on the slide and faintly visible under the microscope, were targeted to confirm the interaction between the MWNTs and FITC-PVLA in a microscopic field. Transmittance light (left column) and fluorescence (right column) images of aggregates of the MWNTs after centrifugation are shown in Figure 3. As shown in Figures 3a and 3b, we were able to observe aggregations but not each needle shape of the 30-MWNTs; the average diameter of the 30-MWNTs determined by SEM was about 30 nm (Figure 1a). These images showed that the aggregates of the 30-MWNTs were coated with FITC-PVLA. By using 200-MWNTs with diameters of about 100–300 nm, the binding of FITC-PVLA to MWNTs was much more clearly shown (Figures 3c and 3d). These images showed that FITC-PVLA was densely localized around the single 200-MWNTs. Probably due to resolution limit of CLSM, needle shapes of 200-MWNTs coated FITC-PVLA were clearly observed than that of 30-MWNTs. Thus 200-MWNTs were used in the following experiments. Although the strength and the amount of PVLA adsorption to MWNTs were not

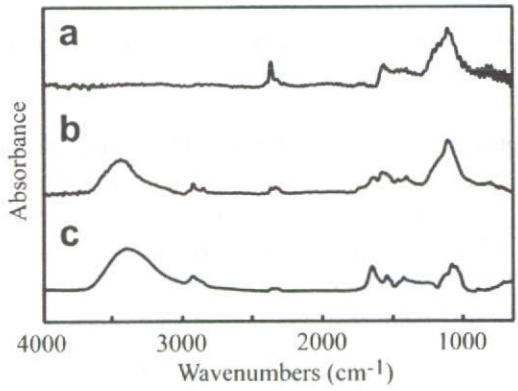

Figure 2. FT-IR spectra of 30-MWNTs (a), the 30-MWNTs coated with PVLA (b), and PVLA (c).

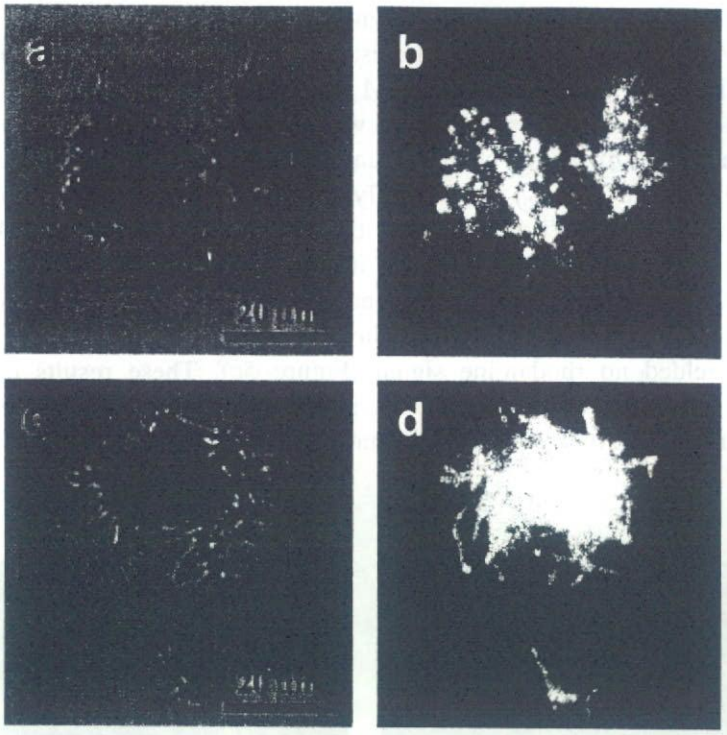

Figure 3. CLSM images of the MWNTs (upper: 30-MWNTs, lower: 200-MWNTs) coated with FITC-PVLA. The left column (a, c) shows images obtained in a transmitted light channel and the right column (b, d) shows images obtained in an FITC channel.

elucidated, PVLA was adsorbed on 30- and 200-MWNTs at sufficient amounts for the modification. Different diameters of MWNTs could effect on PVLA adsorption such as cell adhesion on CNF (35).

We conclude that PVLA is tightly associated with MWNTs because there are interactions between the hydrophobic surface of MWNTs and the hydrophobic polystyrene backbone of PVLA. Binding of a hydrophobic polymer to CNTs is driven by hydrophobic interactions (34) and could be widely utilized for coating CNTs with various carbohydrate-carrying polymers.

Interactions between MWNTs Coated with Carbohydrate-carrying Polymer and Lectins

Carbohydrate chains of glycoproteins, glycolipids and proteoglycans play important roles in recognition phenomena such as fertilization, antigen-antibody reaction, cancer metastasis and infection of viruses and bacteria. These functions are attributable to the biological recognition phenomena induced by lectins and anti-carbohydrate antibodies (28–30).

To estimate the molecular recognition ability of the MWNTs coated with PVLA, interactions with fluorescence-labeled lectins were analyzed using CLSM. Figure 4 shows CLSM images of the 200-MWNTs coated with FITC-PVLA after incubation with Rhod-RCA_{120} [(a) transmitted light channel, (b) FITC channel, and (c) rhodamine channel]. It was found that Rhod-RCA_{120} was densely localized around the 200-MWNTs coated with FITC-PVLA from the rhodamine channel (Figure 4c) and also co-localized with FITC-PVLA adsorbed on the 200-MWNTs from the FITC channel (Figure 4b). In contrast, a control experiment using the combination of Rhod-ConA and the 200-MWNTs coated with FITC-PVLA yielded no rhodamine signal (Figure 5c). These results indicated that the MWNTs coated with PVLA interacted efficiently with the complementary lectin. It is conceivable that the β-galactose moieties of PVLA

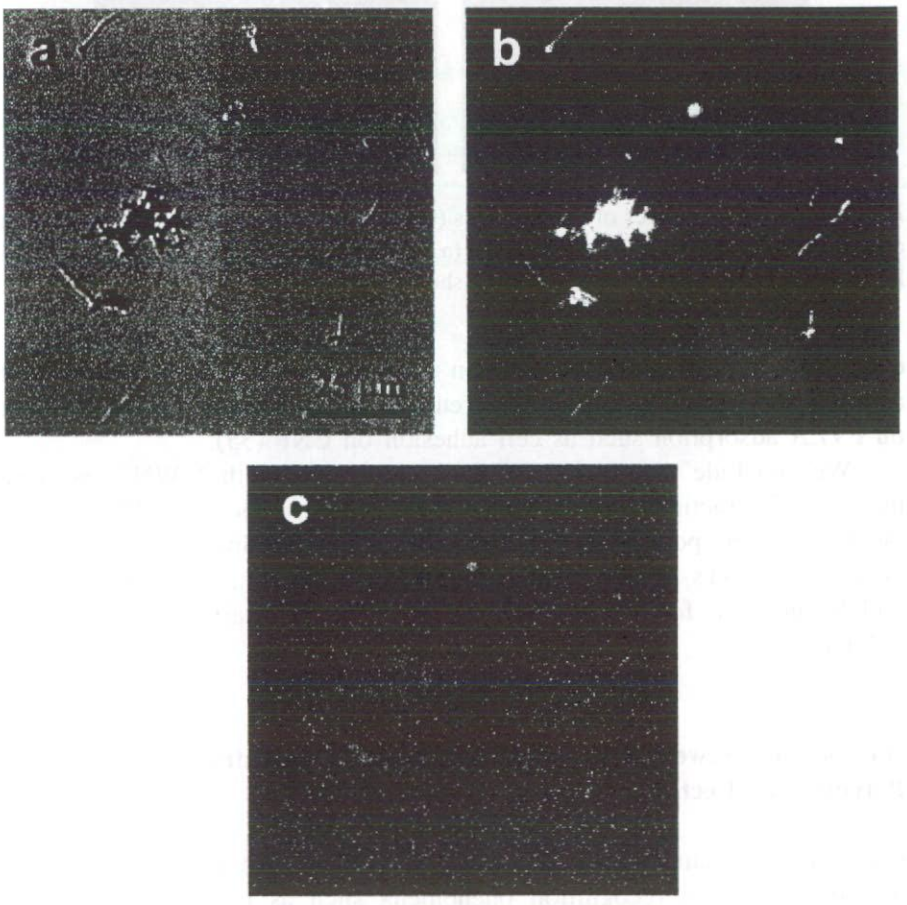

Figure 4. CLSM images of the 200-MWNTs coated with FITC-PVLA after incubation with Rhod-RCA_{120}. (a) Transmitted light channel, (b) FITC channel, and (c) Rhodamine channel.